http://dx.doi.org/10.21611/qirt.2014.144

ON THE HEAT TRANSFER BEHAVIOR OF IMPINGING SYNTHETIC AIR JETS

by C. S. Greco*, A. Ianiro** and G. Cardone*

*Dipartimento di Ingegneria Industriale – Sezione Aerospaziale, Università di Napoli Federico II, 80125 via Claudio 21, Napoli, Italy
**Aerospace Engineering Group, Universidad Carlos III de Madrid, 28911 Av. de la Universidad 30, Laganés, Spain

Abstract

In this work an experimental investigation on the heat transfer between a flat plate and a circular synthetic jet impinging on it is presented. IR thermography is used as temperature transducer in conjunction with the heated thin foil heat transfer sensor. All experiments have been performed at Reynolds number equal to 5,100 while four values of the dimensionless stroke length (L_0/D) equal to 3, 6, 12 and 18 are chosen in order to analyze the four flow regimes defined by McGuinn et al. [13]. For each L_0/D the value of dimensionless nozzle to plate distance (H/D) is varied in order to study all the four stagnation heat transfer regimes defined by Persoons et al. [12] with respect to the ratio $(L_0-L_0^{(f)})/H$, (where $L_0^{(f)}$ is the synthetic jet formation stroke length). The work analyzes the 2D distribution of impingement heat transfer on the impinging plate for any dimensionless stroke length at the same value of $(L_0-L_0^{(f)})/H$. In general, a similarity scaling between different experimental conditions has been found. At low nozzle to plate distance the heat transfer features differ for every flow field configuration and are characterized by the appearance of a minimum in the centre of the impingement and of inner and outer annular maxima.

1. Introduction

Impinging jets are widely recognized and explained in scientific literature [1,2] as one of the most efficient techniques to achieve high heat transfer rate. Recent literature is focusing on the design and optimization of advanced impinging jets devices in order to apply them in particular fields such as electronic cooling. In particular several literature works [3,4,5,6] focus on the study of synthetic impinging jets. Synthetic jets are jets with zero-net-mass flux *"synthesized"* directly from the fluid in the system in which the jet device is embedded. Such a feature obviates the need for an external input piping, making them ideal for low cost and low space applications. A synthetic jet is generated by a membrane oscillation in a cavity which produces a periodic volume change thus pressure variation. As the membrane oscillates, fluid is periodically entrained into and expelled from the orifice. During the injection portion of the cycle the flow field could be considered as one inducted by a sink, which coincides with orifice, while during the expulsion portion of the cycle, a vortex ring can form near the orifice and, under certain operating conditions [7], convects away from the orifice to form a time averaged jet in a limited zone near the jet axis [8]. In synthetic jets literature the stroke length L_0 is the integral of the average velocity at the nozzle exit during the ejection part of the cycle:

$$L_0 = \int_0^{\tau/2} U_a(t)dt \tag{1}$$

and the reference velocity is defined as:

$$U_0 = L_0/\tau \tag{2}$$

where τ is the actuation period and U_a is the exit velocity on the jet axis.
Following Smith and Glezer [8] synthetic jets are characterized by Reynolds number and dimensionless stroke length, which is equal to the inverse of Strouhal number [9] defined as:

$$Re = \rho \cdot U_0 \cdot D \Big/ \mu \tag{3}$$

$$\frac{1}{Sr} = \frac{L_0}{D} \tag{4}$$

http://dx.doi.org/10.21611/qirt.2014.144

where ρ is air density, μ is air dynamic viscosity, D is the nozzle diameter.

Literature works on synthetic jets used as cooling devices has been flourishing only in the last decade. Mahalingam and Glezer [10] studied the design and thermal performance of a heat sink for high power dissipation in electronics enhanced with synthetic jet impingement. The results revealed a case temperature decrease from 71.5 to 36°C with synthetic jets operation and a power dissipation of 20-40% higher with respect to the same heat sink with a fan in the flow rate range of 3-5 cubic feet per minute. Chaudhari et al. [3] carried out experiments on the cooling of a flat plate by using a synthetic jet generated through a circular orifice. Such experiments for Reynolds number in the range 1,500-4,200 and nozzle to plate distance in the range 0-25 D show that the Nusselt number is comparable with that of continuous axisymmetric jets at low Reynolds number (up to 4,000), expecting it to be higher at higher values of Reynolds number. Valiorgue et al. [4] identified two different flow regimes through defining a critical stoke length versus nozzle to plate distance L_0/H equal to 2.5. The heat transfer rate (that obviously increases with Reynolds number increasing) is found to be linearly proportional with L_0/H up to L_0/H = 2.5 than constant for increasing L_0/H values. Literature, moreover, already presents some attempts of obtaining heat transfer correlations for synthetic impinging jets [11,12]. Arik and Icoz [11] established a closed form correlation to predict the heat transfer coefficient as a function of Reynolds number, axial distance, orifice size and jet driving frequency by using experimental data. Such a heat transfer correlation is valid for Re < 2,900, 5 < H/D < 20 and actuation frequency included between 0.16 and 1 times of resonance frequency. They observed that the heat transfer coefficient on a vertical surface increases with the driving voltage, that the cooling performances of synthetic jets peak at their resonance frequencies and that the effect of axial distance on the heat transfer becomes more profound as the jet driving frequency increases. Persoons et al. [12] investigated on the stagnation point heat transfer performance of an axisymmetric synthetic jet versus established steady jet correlations. Such a research led to a general correlation for the stagnation point Nusselt number including the effect of all appropriate scaling parameters: Reynolds number (500 < Re < 1,500), jet to surface spacing (2 < H/D < 16) and stroke length (2 < L_0/D < 40). Based on such a general correlation, Persoons et al. [12] defined four stagnation heat transfer regimes, each one identified by a different range of values acquired by the ratio $(L_0-L_0^{(f)})/H$ (where $L_0^{(f)}$ is the synthetic jet formation stroke length). The flow field features of such four heat transfer regimes were reported by McGuinn et al. [13]. Indeed they carried out high speed PIV and single point hot wire anemometry experiments in order to highlight the dependence of the impinging synthetic jet flow field, and the corresponding surface heat transfer distribution, on the dimensionless stroke length for a wide range of nozzle-to-surface spacing (2 < H/D < 16) and a single Reynolds number (1,500). In such a work McGuinn et al. [13] defined both four free synthetic jet regimes and four impinging synthetic jet flow regimes, whose related heat transfer behaviors are in good agreement with the previous one published by Persoons et al. [12]. Such four free synthetic jet regimes are characterized by: a monotonous increase in vortex strength for $L_0/D \leq 4$, an additional ejected fluid forming a trailing jet following and widening the vortex ring for $4 < L_0/D \leq 8$, a maximum ejection velocity occurring in the trailing jet which destabilizes the vortex ring creating a flow mixing for $8 < L_0/D \leq 16$ and a flow dominated by the trailing jet, defined as the remaining ejected fluid once the primary vortex has been fully formed and propagated, which overtakes the vortex ring resulting in a highly turbulent intermittent jet flow for $L_0/D > 16$. The four impinging synthetic jet flow field regimes are, respectively, featured by: diminishing impingement due to insufficient fluid momentum near the surface for $(L_0-L_0^{(f)})/H \leq 0.5$, optimal impingement for maximum stagnation velocity for $0.5 < (L_0-L_0^{(f)})/H \leq 1$, radial spreading of the jet causing reduction in time-averaged velocity approaching the stagnation point for $1 < (L_0-L_0^{(f)})/H \leq 2$ and regime dominated by trailing jet for $(L_0-L_0^{(f)})/H>2$.

The present work analyzes the heat transfer behavior of each value of the dimensionless stroke length. Under these considerations four different values of dimensionless stroke length (3, 6, 12 and 18) have been chosen for the present work. Such values reflect the four different flow field regimes of a free synthetic jet. For each value of the stroke length several values of nozzle to plate distance have been set in order to achieve the four impinging synthetic jet regimes. In addition also a comparison between the heat transfer distributions for different values of L_0/D at the same impinging synthetic jet regime is provided. The analysis is performed for a Reynolds number equal to 5,100. The impinging wall heat transfer is measured by using IR thermography as temperature transducer coupled with the steady [14] heated thin foil heat transfer sensor. Data is reduced in non-dimensional form as Nusselt number.

2. Experimental setup and data reduction

The experimental apparatus, sketched in fig.1, is practically the same used in Greco et al. [6]. It includes a stainless steel foil (243 mm wide, 715 mm long and 40 μm thick). The foil, constituting the target plate, is steadily and uniformly (in space) heated by Joule effect and is cooled by the synthetic air jet impinging on it. The constant potential difference boundary condition is achieved by using a stabilized DC power supply and two couples of bus bars, made of copper, that are clamped at the shortest sides of the foil. The very large equivalent cross section (weighted with the electrical resistivity) of the bus bars, with respect to that of the heated foil, ensures negligible voltage drop through them. The electrical contact between bus bars and foil is enhanced by putting there an indium wire (about 1mm in diameter). Furthermore, the foil thermal expansion is balanced by the spring-loaded bolts linked to the bus bars and by two spring-loaded insulators [15]. This foil is heated by passing an electric current through it. The target plate is positioned horizontally with the synthetic jets impinging vertically above. This condition is chosen in order to minimize the effects of natural convection on the foil. The single circular synthetic air jet is generated by means of the device shown in Figure 1 that substantially coincides with the device used and already well characterized by the authors [6,16]. A loudspeaker, with diameter is 270 mm, splits the cavity in two sub-cavities with a volume V equal to 2 dm^3. Here one jet is produced from a pipe, attached to one of the two sub-cavities, it has a length L of 210 mm and an inner diameter D of 21 mm.

http://dx.doi.org/10.21611/qirt.2014.144

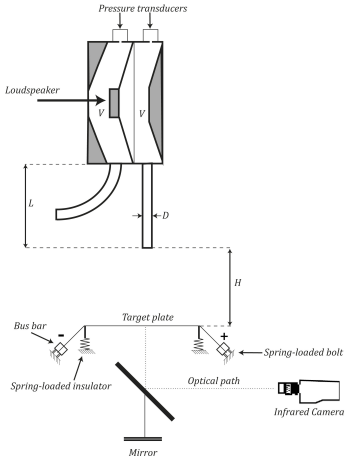

Fig.1 *Sketch of experimental apparatus*

Experiments are performed for four values of the dimesionless stroke length L_0/D (namely 3, 6, 12 and 18). For every value of L_0/D (except of for L_0/D equal to 18 and 12) all the heat transfer regimes are investigated ((L_0-$L_0^{(f)}$)/H equal to 0.4, 0.65, 0.85, 1.4, 1.8, 2.2 and 2.4). For L_0/D equal to 18 and 12 the first two regimes and the first one, respectively, are not realized because of the high required value of H/D (higher than 21) which was not possible to reproduce with the present experimental apparatus and which in our opinion is not of technological interest. All the experiments are performed at the same value of the Reynolds number (5,100).

Reynolds number and dimensionless stroke length are evaluated according to Persoons and O'Donovan [17] from the measured cavity pressure (p_c) with respect to ambient pressure (p_{amb}) applying the unsteady Bernoulli equation for an incompressible flow between a location inside the cavity and a location outside the pipe:

$$dU = \left[\frac{p_c - p_{amb}}{\rho} + \frac{k_{loss} U|U|}{2} \right] \cdot \frac{1}{L} \tag{5}$$

where the head losses k_{loss} in the system are evaluated by comparison with PIV measurements performed by Greco et al. [16]. The used pressure transducers are HSCDRRN002NDAA5 with an accuracy of ±1.5% of the full scale.

The complete synthetic jet device behaves like a mass-spring-damper system with two degrees of freedom [18]. The loudspeaker used in the present experiments (CIARE HS250) has a measured free-space resonance frequency of 25 Hz, a nominal diameter of 208 mm and an equivalent oscillating mass of 56 g. The loudspeaker is supplied with a sinusoidal input signal with a frequency f_1. Such a frequency acquires a different value for each experiment in order to obtain the same Reynolds number varying the stroke length. The input signal is generated by a PC coupled with Analog Discovery™ amplified by an Hi- Fi amplifier (CIARE YSA 300).

An infrared camera (CEPID JADE III 320 x 240 focal plane array) measures the foil surface temperature with a spatial resolution of 1.1 pixels/mm (23 pixels/D). The IR camera is accurately calibrated with a blackbody for the whole measurement range, the noise equivalent temperature level of the camera is about 25 mK and the rms error from the blackbody calibration is less than 0.1 K. The foil surface is coated with high emissivity paint (ε =0.95) in order to increase the accuracy of temperature measurements. In the present case, the IR camera is used in conjunction with the steady state [14] heated thin foil heat transfer sensor. According to the application of the local steady energy balance to the foil, the convective heat transfer coefficient h can be evaluated as:

$$h = \frac{q_j'' - q_r'' - q_k'' - q_n''}{T_w - T_{aw}} \tag{6}$$

with q_j'' the Joule heat flux, q_r'' the radiation heat flux, q_n'' the natural convection heat flux on the rear foil surface, q_k'' the tangential conduction heat flux, T_w the wall temperature and T_{aw} the adiabatic wall temperature.

The surface temperature distribution is measured by viewing the rear face of the foil (i.e. the side opposite to jet impingement) through a mirror, as shown in Figure 1. In fact, since the Biot number ($Bi=hs/\lambda_f$ where s and λ_f are thickness and thermal conductivity of the foil, respectively) is small with respect to unity, the time average temperature can be considered as practically uniform across the foil thickness [19]. Each test run consists of two parts: first, with electric current off, T_{aw} is measured and the so-called "cold images" are recorded; then, electric current on, T_w is measured and the "hot images" are recorded. It has to be outlined that, in order to reduce measurement noise both "hot" and "cold images" are obtained as a time average over 6000 frames.

The net rate of radiation heat loss is estimated as:

http://dx.doi.org/10.21611/qirt.2014.144

$$q_r'' = \varepsilon\sigma\left(T_w^4 - T_a^4\right) \tag{7}$$

where, σ is the Stefan Boltzmann's constant, T_a is the ambient temperature and ε is the total hemispherical emissivity coefficient of the surface (it is found being at worst 45% of q_j'' at $r/D > 5$)
A little more complex is the procedure to compute thermal losses for tangential conduction (that are found being at worst less than 2% of q_j''). In particular, considering the foil plane with axes x and y, thermal losses for tangential conduction can be expressed following Carlomagno et al. [20]:

$$q_k'' = \lambda_f s \cdot \nabla^2 T \tag{8}$$

As suggested by Carlomagno et al. [20], thermal images are filtered before evaluating the Laplacian operator of the surface temperature in order to reduce the effect of the measurement noise. The signal measured by the IR camera, in fact, is affected by measurement noise (noise equivalent temperature difference equal to 25 mK); the effect of noise is reduced by averaging data over the 6000 samples. In order to improve the accuracy a more smooth data is attained with a 7 points second order polynomial filter in space. Losses due to natural convection are mostly related to those of a heated plate facing downward [21]. To calculate exactly these losses in our experimental facility, ad hoc experiments were performed to get an empirical correlation. By applying this correlation thermal losses were evaluated with an accuracy of ±10% of the total value of said losses. The natural convection losses are, at worst, equal to 8% of q_j''. The experimental data are reduced in dimensionless form in terms of time average Nusselt number $Nu=hD/k$ (k is the thermal conductivity of air at film temperature). The present experimental methodology is well assessed in previous works on circular impinging jets [22,23] and synthetic jet [6]. For the present experiments the control parameters and their uncertainty for time average measurements are reported in Table 1. With uncertainty analysis based on the method of Moffat [24], the errors in Reynolds number, considering Eq.(3) and (5) and Table 1 is less than ±3.5% and the error in time average Nusselt number, considering Eq.(6) and Table 1 is less than ±5%.

Table 1 *Control parameters and their uncertainty*

Parameter	Typical value	Typical error
T_{aw}	299 K	0.25 K
T_w	307 – 315 K	0.25 K
T_a	299 K	0.1 K
V	2.1 V	0.021 V
I	35 A	0.35 A
ε	0.95	0.01
q_n''	33.1 W/m^2	3.31 W/m^2
ρ	1.225 Kg/m^3	1.225 10^{-2} Kg/m^3
p_c-p_{amb}	-950 – 950 Pa	7.5 Pa
D	0.021 m	0.1 10^{-3} m
μ	1.8 10^{-5} Pa s	1.8 10^{-7} Pa s
k_{loss}	0.47	0.047
L	0.21 m	0.1 10^{-3} m

3. Results

In this section the heat transfer distribution for each free synthetic jet regime (L_0/D equal to 3, 6, 12 and 18), as defined in McGuinn et al. [13], is presented in the sub section 3.1. The comparison between the heat transfer distribution for different values of L_0/D at the same value of $(L_0-L_0^{(f)})/H$, for $(L_0-L_0^{(f)})/H$ equal to 0.4, 0.65, 0.85, 1.4, 1.8, 2.2 and 2.4, is presented in the sub section 3.2. The law which fits the data and its 2D distribution are presented in the sub section 3.3. The time averaged Nusselt number is presented, in the following figures, as a profile achieved by an azimuthal averaging process, being the investigated phenomenon axisymmetric.

3.1. Effect of L_0/D

The general correlation for the stagnation point heat transfer performance of an impinging synthetic jet is [11]:

$$Nu_0 = 0.171\, Re^{0.686}\, Pr^{0.4}\, f(H)g(L_0) \tag{9}$$

http://dx.doi.org/10.21611/qirt.2014.144

whose range of application is 3 < *H/D* < 16, 2 < L_0/D < 40 and 500 < *Re* < 1500. The stagnation point heat transfer experimental data are compared with such a general correlation. In Figure 2 the experimental data are superimposed to the general correlation with its ±15% uncertainty.. The above correlation matches most part of the experimental data in the entire parameter range to within ±15%. The overall rms normalized deviation, defined as $\delta Nu_0=[n^{-1}\sum((Nu_{0,cor}- Nu_{0,exp})/ Nu_{0,exp})^2]^{1/2}$, is equal to 14.8%. Hence it is possible to assert that, although the experimental Reynolds number (5,100) is higher than the range in which such a correlation is valid, such a general correlation is still valid up to a Reynolds number value of 5,100.

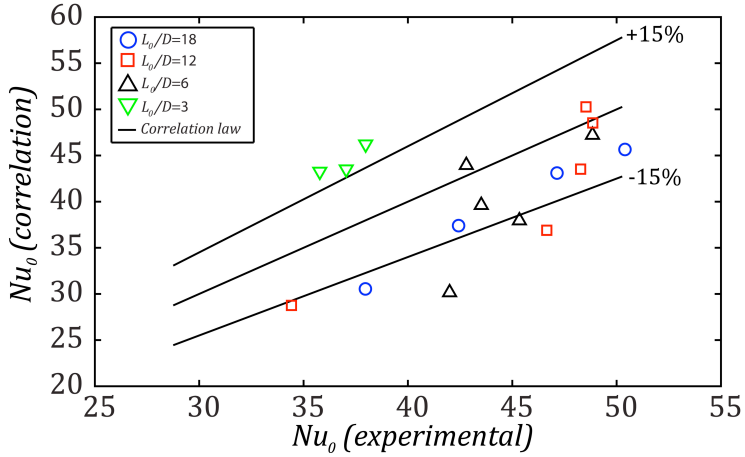

Fig.2 *Comparison between the experimental data (markers) and the general correlation (continuous line) with its ±15% uncertainty*

In Figure 3 a) and b) the Nusselt number profile and the stagnation Nusselt number Nu_0 for the value of L_0/D equal to 18 are reported. Each curve is obtained for a different value of *H/D* in order to realize several $(L_0-L_0^{(f)})/H$. The *H/D* values assumed to perform the requested $(L_0-L_0^{(f)})/H$ are 20.5, 12.5, 9.7, 7.9 and 7.3. One can figure out that, for these values of *H/D*, a decrease in nozzle to plate distance leads to an increase in *Nu* distribution and Nu_0 because the maximum value is attained at *H/D* equal to 6 as seen in Greco et al.[6]. In Figure 3 c) and d) the Nusselt number profile and its stagnation value for L_0/D equal to 12 are depicted. The values of *H/D* employed for this dimensionless stroke length are 17.7, 13.5, 8.2, 6.4, 5.2 and 4.8. For this value of L_0/D the Nusselt number stagnation point increase as nozzle to plate distance decreases. The stagnation point Nusselt number is maximum for *H/D* equal to 5.2 then decreasing nozzle to plate distance also Nu_0 decreases. Such a behavior is similar to the findings obtained by Greco et al.[6] which show a maximum value of the stagnation Nusselt number at *H/D* equal to 6 for a L_0/D equal to approximately 42. In Figure 3 e) and f) *Nu* profile and Nu_0 are shown for a value of L_0/D equal to 6. The used *H/D* values are 13.7, 8.5, 6.5, 3.9, 3, 2.5 and 2.3. In this case Nu_0 has a different behavior with respect to those obtained for stroke length equal to 18 and 12. The stagnation Nusselt number value increases with decrease of *H/D* from 13.7 to 8.5. At *H/D* equal to 8.5 there is a maximum of the stagnation Nusselt number because, as reported in McGuinn et al.[13], for such values of L_0/D and *H/D* the arrival velocity on the plate is maximum. For values of *H/D* lower than 8.5 the stagnation Nusselt number, firstly, begins to decrease and then increases again achieving its maximum value at *H/D* equal to 3. Such a value is constant up to *H/D* equal to 2.5. The presence of the potential core influences the stagnation Nusselt number at *H/D* equal to 2.3. Indeed the stagnation Nusselt number decreases and its maximum value does not occur in the stagnation point. Regarding the Nusselt number distribution one can see that for *H/D* lower than 4 an outer ring shaped region of Nusselt number maxima can be detected. Such a phenomenon is related to the strength of the ring vortex. If the ring vortex has enough vorticity than, as reported in Rohlfs et al. [25], a secondary vortex is created on the plate. Such a secondary vortex causes the unsteady separation and the reattachment of the wall jet and, consequently, the presence of the outer ring shaped region of Nusselt number maxima, as seen by Greco et al.[6]. In Figure 3 g) and h) the Nusselt number profile and its stagnation value for L_0/D equal to 3 are shown. The employed values of *H/D* are 6.2, 3.8, 2.9, 1.8, 1.4, 1.2 and 1.1.The maximum of the stagnation Nusselt number occurs at *H/D* equal to 3.8, remaining approximately constant up to *H/D* equal to 2.9, and then starts decreasing. The decrease is probably ascribed to the presence of the potential core. Indeed for *H/D* values lower than 2.9 the maximum value of Nusselt number does not occur at the stagnation point because, the presence of the potential core, generates the inner ring shaped region of Nusselt number maxima. The first influence of the potential core presence can be inferred from the Nusselt number profile at *H/D* equal to 2.9 where an inner ring shaped region of Nusselt number maxima can be detected at *r/D* equal to about 0.7 Moreover it is possible to highlight that the position (*r/D*) of the maximum Nusselt number increases with *H/D* decrease.

3.2. Impinging synthetic jet heat transfer regimes

Persoons et al. [12] and McGuinn et al.[13] defined four impinging synthetic jets regimes characterized by different values of the $(L_0-L_0^{(f)})/H$. Several values (0.4, 0.65, 0.85, 1.4, 1.8, 2.2 and 2.4) of such a ratio are investigated by using different dimensionless stroke lengths (3, 6, 12 and 18) and nozzle to plate distance. In Figure 4 Nusselt number profiles for each value of $(L_0-L_0^{(f)})/H$ are shown. The Nusselt number profile is normalized using its maximum value (Nu_{max}) and is plotted with

http://dx.doi.org/10.21611/qirt.2014.144

respect to $r/r_{2/3}$ where $r_{2/3}$ is defined as the value of the radius where the Nusselt number achieves the value of $2Nu_{max}/3$. In table 2 the Nu_{max} and the $r_{2/3}$ for each experiment is reported.

Table 2 *Nu_{max} and the $r_{2/3}$ for each experiment*

$(L_0-L_0^{(f)})/H$	L_0/D	H/D	Nu_{max}	$r_{2/3}$ $(10^{-3}m)$
0.4	3	6.2	35.8	44.8
0.4	6	13.7	42.0	60.7
0.65	3	3.8	38.0	44.0
0.65	6	8.5	45.3	57.2
0.65	12	17.7	32.3	91.0
0.85	3	2.9	37.4	48.4
0.85	6	6.5	43.5	59.8
0.85	12	13.5	34.4	84.6
0.85	18	20.5	27.5	105.5
1.4	3	1.8	34.0	58.1
1.4	6	3.9	42.8	71.3
1.4	12	8.2	46.7	51.8
1.4	18	12.5	38.0	71.0
1.8	3	1.4	33.7	59.8
1.8	6	3	49.0	59.8
1.8	12	6.4	48.3	46.4
1.8	18	9.7	42.5	57.3
2.2	3	1.2	33.3	58.1
2.2	6	2.5	48.7	60.7
2.2	12	5.2	48.9	45.5
2.2	18	7.9	47.2	49.1
2.4	3	1.1	32.5	56.3
2.4	6	2.3	44.4	66.0
2.4	12	4.8	48.5	46.4
2.4	18	7.3	50.5	45.5

In Figure 4 a) the two normalized Nusselt number profiles, related to L_0/D equal to 6 and 3, collapse presenting a similar heat transfer behaviour. The same occurs in Figure 4 b) where the curves, associated to L_0/D equal to 12, 6 and 3, show a similar heat transfer shape. In Figure 4 c) the same heat transfer behaviour can be detected for the stroke length L_0/D equal to 18, 12 and 6, but not for the stroke length equal to 3. This curve does not show a monotonic decreasing of the normalized Nusselt number with $r/r_{2/3}$. Such a phenomenon is related to the presence of the potential core which generates, as previously explained, an inner ring shaped region of Nusselt number maxima. In Figures 4 d)-g) the curves of L_0/D equal to 18 and 12 show the same behaviour differently from those related to L_0/D equal to 6 and 3. The Nu/Nu_{max} curve of L_0/D equal to 3 shows the same inner peak which occurred also in Figure 4 c) while the curve of L_0/D equal to 6 shows the outer ring shaped region of Nusselt number maxima.

Such results allow to assert that the heat transfer behavior for any stroke length and nozzle to plate distance is similar in the same regime characterized by the ratio $(L_0-L_0^{(f)})/H$. Nevertheless such a consideration is no longer valid if the value of H/D is comparable to the potential core extension of the synthetic jet, which causes the inner ring shaped region of Nusselt number maxima, or has a value for which the impinging ring vortex has enough vorticity to create the secondary vortex on the wall and, consequently, the outer ring shaped region of Nusselt number maxima.

For L_0/D equal to 3 the maximum value of H/D, causing the inner ring shaped region of Nusselt number maxima, is 2.9. For this value of dimensionless stroke length the outer ring shaped region of Nusselt number maxima was not detected because the generated ring vortex is partially re-ingested during the suction part of the cycle [13] causing a weaker impinging ring vortex.

For L_0/D equal to 6 the outer ring shaped region of Nusselt number maxima is detected for a maximum value of H/D equal to 3.9. For this case the potential core starts influencing the heat transfer behavior at H/D equal to 2.3 but only at H/D equal to 2 the inner ring shaped region of Nusselt number maxima can be detected, as shown in Figure 5 a).

The heat transfer behavior for stroke length equal to 12 and 18 show an inner and outer ring shaped regions of Nusselt number maxima at H/D equal to 4 as reported in Figures 5 b) and c), respectively. This finding is in agreement with the Nusselt number profile obtained by Greco et al.[6] for a single synthetic jet with a L_0/D equal to 42. For this reason it is possible to assert that for values of dimensionless stroke length higher than 12 the value of H/D, at which the inner and outer ring shaped region of Nusselt number maxima occur, is 4.

http://dx.doi.org/10.21611/qirt.2014.144

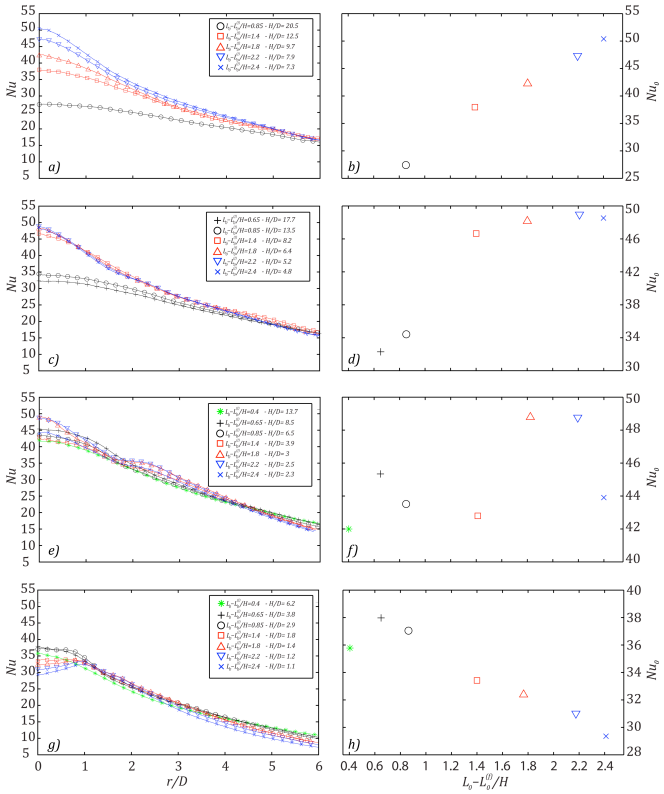

Fig.3 *Nusselt number profile and stagnation Nusselt number for a) - b) L_0/D equal to 18, c) - d) L_0/D equal to 12, e) - f) L_0/D equal to 6 and g) - h) L_0/D equal to 3*

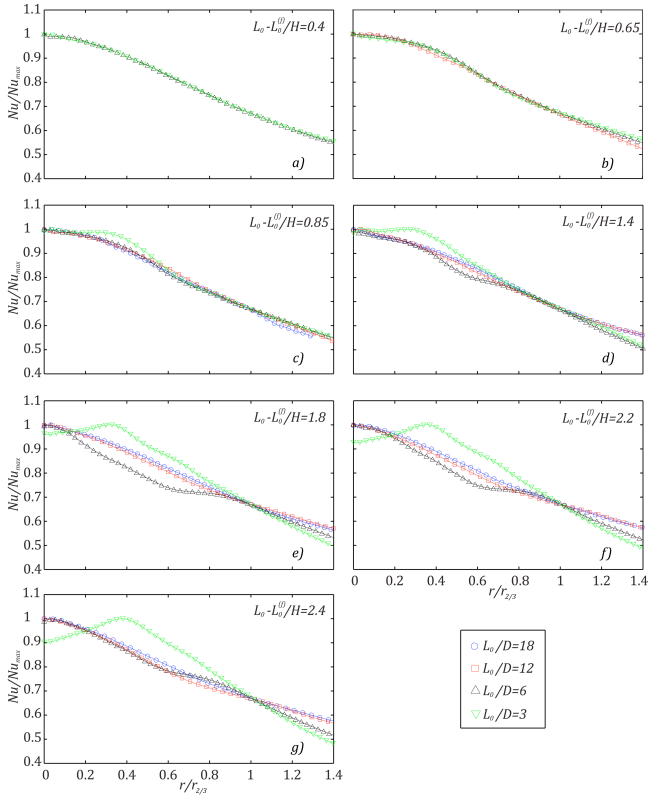

Fig.4 *Normalized Nusselt number profile for each impinging synthetic jet regimes, $(L_0\text{-}L_0^{(f)})/H$, with respect to the dimensionless radius*

http://dx.doi.org/10.21611/qirt.2014.144

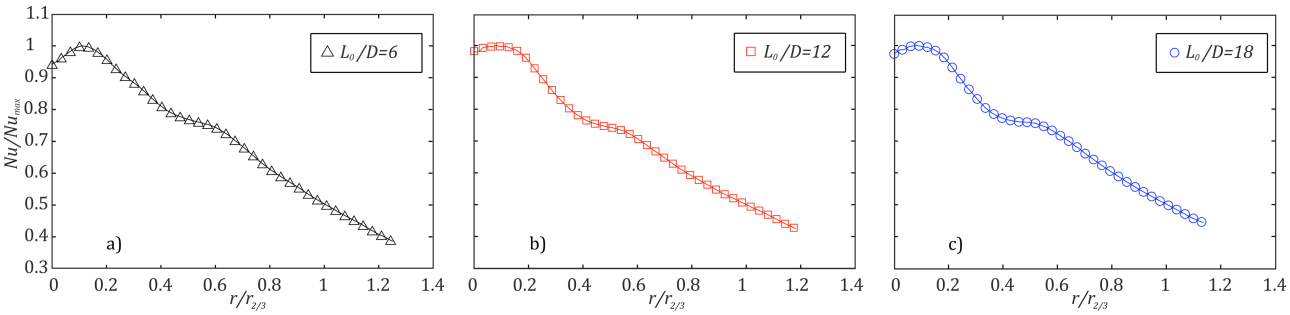

Fig.5 *Detection of inner and outer ring shaped regions of Nusselt number maxima for a) L_0/D equal to 6 at H/D equal to 2, b) L_0/D equal to 12 and c) L_0/D equal to 18 at H/D equal to 4*

3.3. Self similarity in heat transfer behaviour

As previously described the heat transfer profile for each L_0/D at the same $(L_0-L_0^{(f)})/H$ show a similar behaviour except for those cases in which the inner and outer ring shaped region of Nusselt number maxima occur. Such a similarity can be described through a two terms Gaussian law:

$$Nu/Nu_{max} = a_1 \exp(-((r/r_{2/3} - b_1)/c_1)^2) + a_2 \exp(-((r/r_{2/3} - b_2)/c_2)^2) \quad (10)$$

In fig. 6 for each $(L_0-L_0^{(f)})/H$ the collapsing heat transfer behaviour profile are superimposed on the Gaussian law eq 10). One can highlight that such a law fits well the heat transfer shape for each value of $(L_0-L_0^{(f)})/H$. For each $(L_0-L_0^{(f)})/H$ the correlation coefficient R^2, with respect to the Gaussian law Eq.(10), is calculated and in the worst case such a coefficient achieves a value equal to 0.993. All the relevant parameters are summarized in table 3. It is possible to point out that as $(L_0-L_0^{(f)})/H$ increase the normalized Nusselt number profile, firstly, became flat near the stagnation zone ($0.4 < (L_0-L_0^{(f)})/H < 0.85$) and then starts acquiring a sharper form with a more evident peak. In fig.7 a contour of the Gaussian law values with respect to the $(L_0-L_0^{(f)})/H$ (ordinate) and the $r/r_{2/3}$ (abscissa) is depicted. The black dots indicate the values of such a map obtained through the Gaussian law. The entire map is obtained through a local nonlinear least square regression. One can highlight that the area, where a greater heat transfer occur ($Nu/Nu_{max} > 0.9$), shows a maximum at $(L_0-L_0^{(f)})/H$ equal to 0.65, remains constant up to $(L_0-L_0^{(f)})/H$ equal to 0.85 and then starts decreasing. Such a behavior is in agreement with McGuinn et al. [13]. Indeed they find that this regime ($0.5 < (L_0-L_0^{(f)})/H \leq 1$) is characterized by a widening of the vortex ring spreading the impinging fluid over a greater area and reducing fluid velocity. The area with a greater heat transfer became smaller with the increase of the $(L_0-L_0^{(f)})/H$. Such finding lead to the consideration that at high $(L_0-L_0^{(f)})/H$ most part of the heat transfer is localized near the stagnation point. In fact the heat transfer profile, as can be seen in fig.6, became sharper.

Table 3 *Control parameters and their uncertainty*

$(L_0-L_0^{(f)})/H$	a1	b1	c1	a2	b2	c2
0.4	0.72	-1.32	4.60	0.34	-0.05	1.00
0.65	1.32	-3.42	5.10	0.18	0.23	0.64
0.85	0.42	-0.07	0.86	0.61	0.47	2.35
1.4	0.57	-0.18	1.04	0.51	1.01	2.72
1.8	0.11	0.18	0.62	11.71	-16.02	10.01
2.2	0.11	0.11	0.55	2.07	-5.89	6.45
2.4	0.07	0.20	0.39	20.17	-18.01	10.29

http://dx.doi.org/10.21611/qirt.2014.144

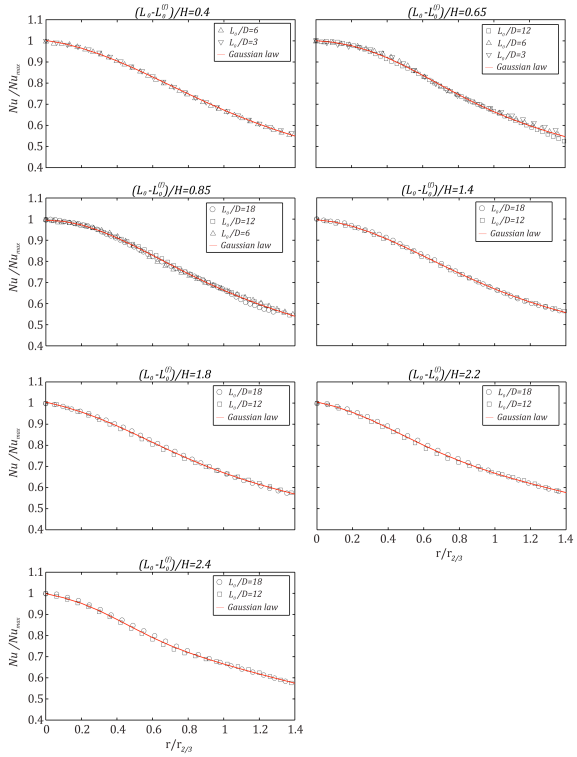

Fig.6 *Heat transfer behavior self similarity for each value of* $(L_0\text{-}L_0^{(f)})/H$

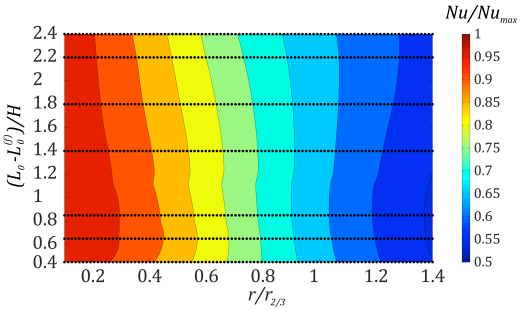

Fig.7 *Gaussian law contour*

4. Conclusions

In this work impinging synthetic jets are experimentally studied at Reynolds number equal to 5,100 and for dimensionless stroke length equal to 3, 6, 12 and 18. The heat transfer on the impinged plate is measured with the steady heated thin foil heat flux sensors using IR thermography as temperature transducer. The analysis is conducted for different values of nozzle to plate distances in order to study the four impinging synthetic jet regimes, defined by McGuinn et al [13], through performing $(L_0\text{-}L_0^{(f)})/H$ equal to 0.4, 0.65, 0.85, 1.4, 1.8, 2.2 and 2.4.

The experimental stagnation Nusselt number, obtained for each L_0/D and H/D, fall within the ±15% uncertainty of the general correlation [12] for the stagnation heat transfer. Such a result allows to consider the general correlation law for the stagnation heat transfer still valid up to Reynolds number equal to 5,100.

The heat transfer behavior for L_0/D equal to 18 and 12 is similar to that obtained by Greco et al. [6] for a synthetic jet characterized by a dimensionless stroke length equal to 42. Indeed such synthetic jets show a maximum stagnation Nusselt number at H/D close to 6 and an inner and outer ring shaped region of Nusselt number maxima for H/D equal to 4.

Instead for a synthetic jet featured by a dimensionless stroke length L_0/D equal to 6 the stagnation Nusselt number shows a first maximum at H/D equal to 8.5 and a second maximum which remains constant between H/D equal to 3 and 2.5. The Nusselt number distribution is characterized by the presence of the outer ring shaped region, which appears for values of H/D lower than 3.9. The inner ring shaped region of Nusselt number maxima is detected for a value of H/D equal to 2. For a dimensionless stroke length equal to 3 the stagnation Nusselt number presents a maximum value at H/D equal to 3.8 which remains approximately constant up to H/D equal to 2.9. For value of H/D equal to 2.9 the inner ring shaped region of Nusselt number maxima can be detected while the outer ring shaped region is not present because of the weak of the vortex ring. In

http://dx.doi.org/10.21611/qirt.2014.144

fact the inner ring shaped region is generated by the presence of the potential core [6,16] while the outer ring shaped region occurs only if the impinging vortex ring has enough strength to generate the secondary vortex on the wall.
A similar heat transfer behavior has been detected for different value of dimensionless stroke length at the same impinging synthetic jet regime ($(L_0-L_0^{(f)})/H$). The normalized Nusselt number profiles collapse in each regimes unless the employed *H/D* has the same extension of the potential core or has a value for which the impinging vortex ring has enough vorticity to create the outer ring shaped region of Nusselt number maxima. In these case such structures modify the heat transfer exchange mechanism causing a different Nusselt number profile. Except for these cases the normalized Nusselt number behavior, for each $(L_0-L_0^{(f)})/H$, can be described by means of a two terms Gaussian law. Such a law allows to assert that at high $(L_0-L_0^{(f)})/H$ the most part of heat transfer occurs near the stagnation point while the largest area interested by an high heat transfer occurs at $0.5<(L_0-L_0^{(f)})/H\leq 1$.

REFERENCES

[1] Martin H., “Heat and Mass Transfer between Impinging Gas Jets and Solid Surfaces”. Advances in Heat Transfer, vol. 13, pp. 1-60, Academic Press, New York, 1977.
[2] Jambunathan K., Lai E., Mossand M.A., Button B.L., “A review of heat transfer data for single circular jet impingement”, International Journal of Heat and Fluid Flow, vol. 13, pp. 106-115, 1992.
[3] Chaudhari M., Puranik B., Agrawal A., “Heat transfer characteristics of synthetic jet impingement cooling”, International Journal of Heat and Mass Transfer, vol. 53, pp. 1057-1069, 2010.
[4] Valiorgue P., Persoons T., McGuinn A., Murray D.B., “Heat transfer mechanisms in an impinging synthetic jet for small jet-to-surface spacing”, Experimental Thermal and Fluid Science, vol. 33, pp.59 7-603, 2009.
[5] Bhapkar U.S., Srivastava A., Agrawal A., “Acoustic and heat transfer aspects of an inclined impinging synthetic jet”, International Journal of Thermal Science, vol. 74, pp. 145-155, 2013.
[6] Greco C.S., Ianiro A. and Cardone G., “Time and phase average heat transfer in single and twin circular synthetic impinging air jets”, International Journal of Heat and Mass Transfer, vol. 73, pp. 776 - 788, 2014.
[7] Holman R., Utturkar Y., Mittal R., Smith B.L., Cattafesta L., “Formation criterion for synthetic jets”, AIAA Journal, vol. 43(10), pp. 2110-2116, 2005.
[8] Smith B.L., Glezer A., “The formation end evolution of synthetic jets”, Physics of Fluids, vol. 10(9), pp. 2281-2297, 1998.
[9] Cater J.E., Soria J., “The evolution of round zero-net-mass-flux jets”, Journal of Fluid Mechanic, vol. 472, pp. 167-200, 2002.
[10] Mahalingam R., Glezer A., “Design and thermal characteristic of a synthetic jet ejector heat sink”, Journal of Electronic Packaging, vol. 127, pp. 172-177, 2005.
[11] Arik M., Icoz T., “Predicting heat trasnfer from unsteady synthetic jets”, Journal of Heat Transfer, vol. 134, pp. 1-8, 2012.
[12] Persoons T., McGuinn A., Murray D.B.,” A general correlation for the stagnation point Nusselt number of an axisymmetric impinging synthetic jet”, International Journal of Heat and Mass Transfer, vol. 54, pp. 3900-3908, 2011.
[13] McGuinn A., Farrelly R., Persoons T., Murray D.B., “Flow regime characterisation of an impinging axisymmetric synthetic jet”, Experimental Thermal and Fluid Science, vol. 47, pp. 241–251, 2013.
[14] Carlomagno G.M., Cardone G., “Infrared thermography for convective heat transfer measurements”, Experiments in Fluids, vol. 49, pp. 1187-1218, 2010.
[15] Imbriale M., Panelli M, Cardone G. “Heat transfer enhancement of natural convection with ribs”, QIRT Journal, vol. 9(1), pp. 55-67, 2012.
[16] Greco C.S., Ianiro A., Astarita T., Cardone G., “On the near field of single and twin circular synthetic air jets”, International Journal of Heat and Fluid Flow, vol. 44, pp. 41–52, 2013.
[17] Persoons, T., O'Donovan, T.S., “A pressure-based estimate of synthetic jet velocity”, Physics of Fluids, vol. 19 (12) , art. no. 128104, 2007.
[18] Persoons T., “General reduced-order model to design and operate synthetic jet actuators”, AIAA Journal, vol. 50, pp. 916-927, 2012.
[19] Astarita T., Carlomagno G. M., “Infrared thermography for thermo-fluid-dynamics”, Springer, 2013.
[20] Carlomagno, G.M., Discetti S., Astarita T., “Experimental assessment of a new heat flux sensor for measuring convective heat transfer coefficients”, QIRT Journal, vol. 8(1), pp. 37-49, 2011.
[21] McAdams, W.H., “Heat Transmission”, 3rd Ed. McGraw-Hill, New York, NY, 1954.
[22] Violato D., Ianiro A., Cardone G., Scarano F., “Three-dimensional vortex dynamics and convective heat transfer in circular and chevron impinging jets”, International Journal of Heat and Fluid Flow, vol. 37, pp. 22–36, 2012.
[23] Ianiro A., Cardone G., “Heat transfer rate and uniformity in multichannel swirling impinging jets”, Applied and Thermal Engineering, vol. 49, pp. 89-98, 2012.
[24] Moffat R.J., “Describing the uncertainties in experimental results”, Experimental Thermal and Fluid Science, vol. 1, pp. 3-17, 1988.
[25] Rohlfs W., Haustein H.D., Garbrecht O., Kneer R., “Insights into local heat transfer of a submerged impinging jet: Influence of local flow acceleration and vortex-wall interaction”, International Journal of Heat and Mass Transfer, vol. 55, pp. 7728-7736, 2012.